

A new model of cosmogenic production of radiocarbon ^{14}C in the atmosphere

Gennady A. Kovaltsov^a, Alexander Mishev^{b,c}, Ilya G. Usoskin^{b,d,*}

^a*Ioffe Physical-Technical Institute, St. Petersburg, Russia*

^b*Sodankylä Geophysical Observatory (Oulu unit), University of Oulu, Finland*

^c*Institute for Nuclear Research and Nuclear Energy, Bulgarian Academy of Sciences, 72 Tzarigradsko chaussee, 1784 Sofia, Bulgaria*

^d*Dept. of Physical Sciences, University of Oulu, Finland*

Abstract

We present the results of full new calculation of radiocarbon ^{14}C production in the Earth atmosphere, using a numerical Monte-Carlo model. We provide, for the first time, a tabulated ^{14}C yield function for the energy of primary cosmic ray particles ranging from 0.1 to 1000 GeV/nucleon. We have calculated the global production rate of ^{14}C , which is 1.64 and 1.88 at/cm²/sec for the modern time and for the pre-industrial epoch, respectively. This is close to the values obtained from the carbon cycle reservoir inventory. We argue that earlier models overestimated the global ^{14}C production rate because of outdated spectra of cosmic ray heavier nuclei. The mean contribution of solar energetic particles to the global ^{14}C is calculated as about 0.25% for the modern epoch. Our model provides a new tool to calculate the ^{14}C production in the Earth's atmosphere, which can be applied, e.g., to reconstructions of solar activity in the past.

Keywords:

cosmic rays, Earth's atmosphere, cosmogenic isotopes, radiocarbon ^{14}C

1. Introduction

Radiocarbon ^{14}C is a long-living (half-life about 5730 years) radioactive nuclide produced mostly by cosmic rays in the Earth's atmosphere. Soon after production, it gets oxidized to $^{14}\text{CO}_2$ and in the gaseous form takes part in the complex global carbon cycle (Bolin et al., 1979). Radiocarbon is important not only because it is used for dating in many applications (e.g., Dorman, 2004; Kromer, 2009), but also because it forms a primary method of paleo-reconstructions of solar activity on the millennial time scales (e.g., Stuiver and Quay, 1980; Stuiver and Braziunas, 1989; Bard et al., 1997; Muscheler et al., 2007). An essential part of the solar activity reconstruction from radiocarbon data is computation of ^{14}C production by cosmic rays in the Earth's atmosphere. First such computations were performed in the 1960–1970s (e.g., Lingenfelter, 1963; Lingenfelter and Ramaty, 1970; Light et al., 1973; O'Brien, 1979) and were based on simplified numerical or semi-empirical methods. Later, full Monte-Carlo simulations of

*Corresponding author, e-mail: ilya.usoskin@oulu.fi
Authors are listed in the alphabetical order

11 the cosmic-ray induced atmospheric cascade had been performed (Masarik and Beer, 1999; Masarik and Beer, 2009).
12 Most of earlier models, including O'Brien (1979) and Masarik and Beer (1999) deal with a prescribed functional
13 shape of the galactic cosmic ray spectrum, which makes it impossible to be applied to other types of cosmic ray
14 spectra, e.g., solar energetic particles, supernova explosions, etc. A flexible approach includes calculation of the yield
15 function (the number of cosmogenic nuclei produced in the atmosphere by the primary cosmic rays of the given type
16 with the fixed energy and unit intensity outside the atmosphere), which can be convoluted with any given energy
17 spectrum of the primary cosmic rays (e.g., Webber and Higbie, 2003; Webber et al., 2007; Usoskin and Kovaltsov,
18 2008; Kovaltsov and Usoskin, 2010). This approach can be directly applied to, e.g., a problem of the signatures of
19 extreme solar energetic particle events in the cosmogenic nuclide data, which is actively discussed (e.g., Usoskin et al.,
20 2006; Hudson, 2010; LaViolette, 2011). Some earlier models (Lingenfelter, 1963; Castagnoli and Lal, 1980) provide
21 the ^{14}C yield function however it is limited in energy. Moreover, different models give results which differ by up to
22 50% from each other, leading to large uncertainty in the global ^{14}C production rate. Therefore, the present status is
23 that models providing the yield function are 30–50 years old **and have large uncertainties**.

24 In addition, there is a systematic discrepancy between the results of theoretical models for the ^{14}C production
25 and the global average ^{14}C production rate obtained from direct measurements of the specific $^{14}\text{CO}_2$ activity in the
26 atmosphere and from the carbon cycle reservoir inventory. While earlier production models predict that the global
27 average pre-industrial production rate should be 1.9–2.5 atoms/cm²/sec, estimates from the carbon cycle inventory
28 give systematically lower values ranging between 1.6 and 1.8 atoms/cm²/sec (Lingenfelter, 1963; Lal and Suess, 1968;
29 Damon and Sternberg, 1989; O'Brien et al., 1991; Goslar, 2001; Dorman, 2004). This discrepancy is known since
30 long (Lingenfelter, 1963) but is yet unresolved (Goslar, 2001).

31 In this work we redo all the detailed Monte-Carlo computations of the cosmic-ray induced atmospheric cascade
32 and the production of ^{14}C in the atmosphere to resolve the problems mentioned above. In Section 2 we describe the
33 numerical model and calculation of the radiocarbon production. In Section 3 we compare the obtained results with
34 earlier models. In Section 4 we apply the model to calculate the ^{14}C production by galactic cosmic rays and solar
35 energetic particle events for the last solar cycle. Conclusions are presented in Section 5.

36 **2. Calculation of the ^{14}C production**

37 Energetic primary cosmic ray particles, when entering the atmosphere, collide with nuclei of the atmospheric
38 gases initiating a complicated nucleonic cascade (also called shower). Here we are interested primarily in secondary
39 neutrons whose distribution in the atmosphere varies with altitude, latitude, atmospheric state and solar activity. Neu-
40 trons are produced in the atmosphere through multiple reactions including high-energy direct reactions, low-energy
41 compound nucleus reactions and evaporation of neutrons from the final equilibrium state. Most of neutrons with en-
42 ergy below 10 MeV are produced as an evaporation product of excited nuclei, while high-energy neutrons originate as
43 knock-on neutrons in collisions or in charge exchange reactions of high-energy protons. While knock-on neutrons are

44 mainly emitted in the forward direction (viz. downwards), evaporated neutrons of lower energy are nearly isotropic.
 45 Radiocarbon ^{14}C is a by-product of the nucleonic cascade, with the main channel being through capture of secondary
 46 neutrons by nitrogen: $\text{N}^{14}(\text{n},\text{p})\text{C}^{14}$. Other channels (e.g., via spallation reactions) contribute negligibly, but are also
 47 considered here.

48 We have performed a full Monte Carlo simulation of the nucleonic component of the cosmic ray induced atmo-
 49 spheric cascade, using the Planetocosmic code (Desorgher et al., 2005) based on GEANT-4 toolkit for the passage of
 50 particles through matter (Geant4 Collaboration et al., 2003) (see details in Appendix). The secondary particles were
 51 tracked through the atmosphere until they undergo reactions with an air nucleus, exit the atmosphere or decay. In
 52 particular, secondary neutrons were traced down to epi-thermal energy. Simulations are computationally intensive.
 53 Simulations of single energies (ranging from 0.1 to 1000 GeV/nuc) were conducted, to determine the resulting flux of
 54 secondary neutrons. Since the calculations require very large computational time to keep the statistical significance
 55 of the results for low energies, we applied an analytical approach for atmospheric neutrons with energy below 10
 56 eV (see details in Appendix). Cross-sections have been adopted from the Experimental Nuclear Reaction Database
 57 (EXFOR/CSISRS) <http://www.nndc.bnl.gov/exfor/exfor00.htm>. The number of simulated cascades induced by pri-
 58 mary CR particles was chosen as $10^5 - 10^6$ to keep the statistical stability of the results at a reasonable computational
 59 time. Computations were carried out separately for primary protons and α -particles. Because of the similar rigid-
 60 ity/energy ratio, nuclei with $Z > 2$ were considered as effectively α -particles with the scaled number of nucleons (cf.
 61 Usoskin and Kovaltsov, 2008).

62 As the main result of these detailed computations we calculated the ^{14}C yield function. The yield functions for pri-
 63 mary protons and α -particles are tabulated in Table A.1 and shown in Fig. A.1 (the energy range above 100 GeV/nuc
 64 is not shown). Note that the yields (per nucleon with the same energy) are identical for protons and α -particle, viz.
 65 an α -particle is identical to four protons, at energies above 10 GeV/nuc. Details of the computations are given in
 66 Appendix Appendix A. All further calculations are made using these yield functions.

67 In order to compute the ^{14}C production q in the atmosphere at a certain place and conditions/time, one can use the
 68 following method:

$$q(t) = \sum_i \int_{E_{ic}}^{\infty} Y_i(E) J_i(E, t) dE, \quad (1)$$

69 where E is the particle's kinetic energy per nucleon, J_i is the spectrum of primary particles of type i on the top of the
 70 atmosphere, E_{ic} in GeV/nucleon is the kinetic energy per nucleon corresponding to the local geomagnetic rigidity
 71 cutoff P_c in GV.

$$P_c = \frac{A_i}{Z_i} \sqrt{E_{ic} (E_{ic} + 2 E_r)}, \quad (2)$$

72 where $E_r = 0.938$ GeV/nucleon is the proton's rest mass. Summation is over different types of the primary cosmic
 73 ray nuclei with charge Z_i and mass A_i numbers. The local geomagnetic rigidity cutoff is roughly defined via the
 74 geomagnetic latitude λ_G of the location as following (Elsasser et al., 1956)

$$P_c [\text{GV}] = 1.9 \cdot M \cdot \cos^4 \lambda_G, \quad (3)$$

75 where M is the dipole moment in units of [10^{22} A m²] of the Earth's magnetic field. Although this approximation
 76 may slightly $\leq 2\%$ overestimate the ^{14}C production (O'Brien, 2008), it is sufficient to study the global cosmic ray flux
 77 (Dorman, 2009; Clem et al., 1997). The global production Q of radiocarbon is defined as the spatial global average
 78 of the local production q (both quantities give the number of ^{14}C nuclei produced per second per cm² of the Earth's
 79 surface). For the isotropic flux of primary particles in the interplanetary space (the level of anisotropy for galactic
 80 cosmic rays is usually smaller than 1%) the global production can be written as:

$$Q(t) = \sum_i \int_0^\infty Y_i(E) J_i(E, t) (1 - f(E)) dE, \quad (4)$$

81 where the function

$$f(E) = \begin{cases} \sqrt{1 - \sqrt{P(E)/(1.9 \cdot M)}}, & \text{if } P \leq 1.9 \cdot M \\ 0, & \text{if } P > 1.9 \cdot M \end{cases} \quad (5)$$

82 corresponds to $\sin(\lambda_G)$ and accounts for the spatial average with the effect of the geomagnetic cutoff.

83 Substituting any particular particle spectrum J_i into Eq. 4 one can evaluate the ^{14}C production rate for different
 84 populations of cosmic rays, e.g., galactic cosmic rays (GCR), solar energetic particles (SEP), or more exotic sources
 85 like a nearby supernova explosion.

86 First we consider the main source of ^{14}C , GCR modulated by the solar activity, using the standard approach. The
 87 energy spectrum of GCR particles of type i at 1 AU, J_i , is defined by the local interstellar spectrum (LIS), $J_{\text{LIS},i}$, and
 88 the modulation potential ϕ as (see the formalism in Usoskin et al., 2005):

$$J_i(E, \phi) = J_{\text{LIS},i}(E + \Phi_i) \frac{(E)(E + 2E_r)}{(E + \Phi_i)(E + \Phi_i + 2E_r)}, \quad (6)$$

89 where $\Phi_i = (eZ_i/A_i)\phi$. The modulation potential ϕ is the variable related to solar activity, that parameterizes the shape
 90 of the modulated GCR spectrum. The fixed function $J_{\text{LIS}}(T)$ is not exactly known and may affect the absolute value of
 91 ϕ (e.g., Usoskin et al., 2005; Webber and Higbie, 2009; Herbst et al., 2010; O'Brien, 2010). Thus, the exact model of
 92 LIS must be specified together with the values of ϕ . Here we use, as earlier, the proton LIS in the form (Burger et al.,
 93 2000; Usoskin et al., 2005):

$$J_{\text{LIS}}(E) = \frac{1.9 \times 10^4 \cdot P(E)^{-2.78}}{1 + 0.4866 P(E)^{-2.51}}, \quad (7)$$

94 where $P(E) = \sqrt{E(E + 2E_r)}$, J and E are expressed in units of particles/(m² sr s GeV/nucleon) and in GeV/nucleon,
 95 respectively. Here we consider two species of GCR separately: protons and heavier species, the latter including
 96 all particles with $Z > 1$ as α -particles with $Z/A = 0.5$ scaled by the number of nucleons. Heavier species should be
 97 treated separately as they are modulated in the heliosphere and Earth's magnetosphere differently, compared to protons
 98 because of the different Z/A ratio. Here we consider the nucleonic ratio of heavier particles (including α -particles) to
 99 protons in the interstellar medium as 0.3 (Webber and Higbie, 2003; Nakamura et al., 2010).

100 The global ^{14}C production Q by GCR depends on two parameters, the solar magnetic activity quantified via the
 101 modulation potential ϕ and the Earth's geomagnetic field (its dipole moment M). The dependence is shown in the

102 upper panel of Fig. A.2. One can see that both parameters are equally important, and the knowledge of the geomagnetic
103 field is very important (Snowball and Muscheler, 2007). In the lower panel, three cuts of the upper panel are shown
104 to illustrate the effect of solar activity on Q , for the fixed geomagnetic field, corresponding to the modern conditions
105 $M = 7.8 \cdot 10^{22} \text{ A m}^2$, as well as maximum (10^{23} A m^2) and minimum ($6 \cdot 10^{22} \text{ A m}^2$) dipole strength over the last
106 ten millennia of the Holocene (Korte et al., 2011). The response of Q to changes of the geomagnetic field during the
107 Holocene is within $\pm 15\%$. However, the global ^{14}C would be nearly doubled during an inversion of the geomagnetic
108 field (viz. $M \rightarrow 0$). The modulation potential ϕ varies between about 300 and 1500 MV within a modern high solar
109 cycle (Usoskin et al., 2011), and can be as low as about 100 MV during the Maunder minimum (McCracken et al.,
110 2004; Usoskin et al., 2007; Steinhilber et al., 2008). Thus, changes of the solar modulation can also lead to a factor of
111 2–3 variability on the global ^{14}C production rate.

112 Next we investigated the sensitivity of Q to the energy of GCR. In Fig. A.3 we show the relative cumulative
113 production of ^{14}C , viz. the fraction of the total production caused by primary cosmic rays with energy below the given
114 value E , as a function of E for different conditions. Often the median energy (the energy which halves the production)
115 is used as a characteristic energy (e.g., Lockwood and Webber, 1996), which is the crossing of the curves in Fig. A.3
116 with the horizontal dashed line. One can see that the median energy of ^{14}C production slightly changes with the level
117 of solar activity, varying between 4 and 10 GeV/nuc corresponding to the Maunder minimum and the maximum of a
118 strong solar cycle, respectively. The sensitivity of Q to the energy of GCR is close to that of a sea-level polar neutron
119 monitor (cf. Beer, 2000). Slightly different shape of the neutron monitor cumulative response is due to the fact that it
120 is ground-based while ^{14}C is produced in the entire atmosphere.

121 As an example, we calculated the ^{14}C production predicted by the model for the last 60 years (see Fig. A.4) using
122 the GCR modulation, reconstructed from the ground-based network of neutron monitors (Usoskin et al., 2011), and
123 IGRF (International Geomagnetic Reference Field – <http://www.ngdc.noaa.gov/IAGA/vmod/igrf.html>) model of the
124 Earth’s magnetic field. The mean radiocarbon production for that period (1951–2010) is $Q = 1.64 \text{ atom/cm}^2/\text{sec}$, with
125 the variability by a factor of two between 1.1 (in 1990 solar maximum) and 2.2 (in 2010 solar minimum) $\text{atom/cm}^2/\text{sec}$.

126 The mean ^{14}C production for the pre-industrial period (1750–1900) calculated using the GCR modulation recon-
127 struction by Alanko-Huotari et al. (2007) and paleomagnetic data by Korte et al. (2011) is $1.88 \text{ atom/cm}^2/\text{sec}$ which
128 is essentially lower than those reported in earlier works ($1.9\text{--}2.5 \text{ atom/cm}^2/\text{sec}$) and closer to the values obtained from
129 the carbon cycle inventory ($1.6\text{--}1.8 \text{ atom/cm}^2/\text{sec}$) – see Introduction. This values can be further $\approx 2\%$ lower because
130 of the used geomagnetic cut-off approach (O’Brien, 2008).

131 3. Comparison with earlier models

132 In Fig. A.1 we compare our present results with the yield functions calculated earlier (see the Figure caption for
133 references). Our results are consistent with most of the earlier calculations (LR70 and DV91) within 10-20%. The
134 CL80 yield function is not independently calculated but modified from LR70. While it is formally given for protons it

135 effectively includes also α -particles via scaling, thus being systematically higher than the other yield functions. Note
136 that all the earlier computations of the yield function were limited in energy so that the upper considered energy of
137 primary cosmic rays was from several to 50 GeV/nuc. On the other hand, contribution of higher energy cosmic rays
138 is significant and may reach half of the total ^{14}C production (see Fig. A.3). Here we present, for the first time, the ^{14}C
139 yield function calculated up to TeV/nuc energy. Contribution from the higher energies is negligible because of the
140 steep spectrum of GCR.

141 Next we perform a more detailed comparison with the most recent ^{14}C production model by Masarik and Beer
142 (2009, - MB09), who also used a GEANT-4 Monte-Carlo simulation tool. Since MB09 did not calculate the yield
143 function, we use another way of comparison, via computing the global averaged ^{14}C production rate, as illustrated in
144 Fig. A.5. Our present result (black curve Q) in the Figure is systematically lower than that given by MB09 (big dots)
145 by 25-30%. We suspect that the discrepancy arises from that Masarik and Beer (2009) calculated the ^{14}C production
146 for a prescribed GCR spectrum in the form given by (Garcia-Munoz et al., 1975; Castagnoli and Lal, 1980), which
147 is different from the spectrum we use here (adopted from Usoskin et al., 2005; Herbst et al., 2010). Thus, in order to
148 compare our results with those of MB09, we repeat our computations based on Eq. 1 to compute the global production
149 Q^* but using the same spectrum as MB09. The result for Q^* is shown by the grey curves in Fig. A.5. The overall
150 agreement is within 5% but Q^* value is systematically higher than that of MB09. The 5% difference can be related
151 to the slightly different numerical scheme and also to the fact that MB09 treated an α -particle as four protons while
152 we simulated them straightforwardly. In addition, the way of considering the geomagnetic shielding by MB09 is
153 simplified (scaling) compared to our consideration (direct computations). We also compared the proton contributions
154 (two dashed curves in Fig. A.5) to Q for the GCR spectrum discussed here (Eq. 6) and that used in MB09. The
155 curves are nearly identical, suggesting that the difference in the used proton spectra is small and cannot be a cause
156 for the observed systematic difference. We however notice a great difference between the α - (and heavier) particle
157 spectra used here and in MB09. MB09 assumed of 12% for α - and 1% for heavier particle fraction in LIS (leading
158 to ≈ 0.64 nucleonic ratio between heavier species to protons in GCR) basing on the data from Simpson (1983). On
159 the other hand, modern measurements (e.g., AMS, PAMELA) suggest that α -particles above 10 GeV/nuc contribute
160 5–6% (in particle number) to LIS of GCR leading to the nucleonic fraction of heavier species to protons of the
161 order of 0.25-0.3 outside the heliosphere (e.g. Alcaraz et al., 2000a,b; Adriani et al., 2011; Webber and Highbie, 2003;
162 Nakamura et al., 2010), viz. half of that assumed by MB09. Therefore, while we agree with MB09 in calculations
163 of proton contribution into Q , they overestimate ^{14}C production by heavier species of GCR, using outdated spectra.
164 This explains why the earlier results by MB99 and MB09 of ^{14}C production are systematically higher than our present
165 result.

166 Next we compare predictions of our model with other models' results for specific periods of time as shown in
167 Fig. A.6 (exact data sets used are mentioned in the Figure caption). One can see that our model predicts systematically
168 lower production rates than most of other models, except of the model by O'Brien (1979) and O'Brien et al. (1991).
169 On the other hand, our yield function is generally consistent with others (Fig. A.1), indicating that the difference must

170 be related to the treatment of incoming GCR particle spectra and/or geomagnetic shielding and not to the atmospheric
171 cascade simulations. Models other than that by O'Brien (1979) were based on theoretical calculations and included
172 outdated overestimated abundance of α -particles, which explains the difference as discussed above. Therefore, we
173 conclude that our model more correctly calculates the ^{14}C production as it agrees with the empirically-based models.

174 4. ^{14}C production by solar energetic particles

175 We also calculated production of radiocarbon by solar energetic particles (SEP), because presently there is a wide
176 range of the results (e.g., Lingenfelter and Ramaty, 1970; Usoskin et al., 2006; Hudson, 2010; LaViolette, 2011).
177 Here we compute the expected production of ^{14}C by the major known SEP events since 1951, using our calculated
178 yield function (Table A.1) and SEP event-integrated spectra as reconstructed by Tylka and Dietrich (2009). The
179 corresponding production rate is shown by big open dots in Fig. A.4 reduced to the monthly mean values. One can see
180 that only a few SEP events can produce significant enhancements in ^{14}C production ($\approx 70\%$ in the monthly mean for
181 the SEP event of 23-Feb-1956, 40% for 12-Nov-1960, 35% for two events in Oct-1989 and $\approx 20\%$ for 29-Sep-1989).
182 However, when applied to the annual time scale (the standard tree-ring time resolution), it gives only a few percent
183 effect for years of maximum solar activity and about 0.25% of the total contribution over the considered period. This is
184 consistent with the earlier results by Lingenfelter and Ramaty (1970) (1.1% mean contribution of SEP into the global
185 ^{14}C production for 1954–1965, our model for the same period gives 0.8%) and by Usoskin et al. (2006) (0.2% for
186 1955–2005). Note that MB09, however, gives much smaller value of 0.02% for the SEP contribution to the global
187 mean ^{14}C production, which is probably caused by the neglect of the atmospheric cascade (and thus neutron capture
188 channel) caused by SEPs (cf. Masarik and Reedy, 1995).

189 5. Conclusions

- 190 • We have performed full new calculation, based on a detailed Monte-Carlo simulation of the atmospheric cascade
191 by a GEANT-4 tool PLANETOCOSMIC, of the ^{14}C yield function. This is the first new calculation of the yield
192 function since 1960-1970's, using modern techniques and methods, and the yield function is, for the first time
193 ever, directly computed up to the energy of 1000 GeV/nuc (earlier models were limited to a few tens GeV/nuc
194 and extrapolated to higher energies). Our newly computed yield function gives the results which are in good
195 agreement with O'Brien (1979) and consistent with most of the earlier models, within 10-20%.
- 196 • We have calculated, using the new model and improved spectra of cosmic rays, the global production of ^{14}C ,
197 which appears to be significantly lower than earlier estimates and closer to the values obtained from the carbon
198 cycle inventory. The calculated modern global production rate is 1.64 atom/cm²/sec, and the preindustrial rate
199 (1750–1900 AD) is 1.88 atom/g/cm², which is essentially lower than earlier estimates of 2–2.5 atom/cm²/sec.

- 200 • We explain that the earlier models (including a recent model by Masarik and Beer (2009)) overestimate the
201 contribution of α -particle and heavier GCR species to the ^{14}C production, because of the use of outdated
202 spectra.
- 203 • We have calculated, on the basis of the new model, contribution to the global ^{14}C production by SEP events,
204 using updated energy spectra reconstructions by Tylka and Dietrich (2009). The mean contribution of the SEPs
205 for the last 50 years is estimated to be $\approx 0.25\%$ of the total production.
- 206 • The present model provides an improved tool to calculate the ^{14}C production in the Earth's atmosphere. Using
207 the absolutely dated ^{14}C calibration curve (Reimer et al., 2009), one can reconstruct the variability of cosmic
208 rays in the past (e.g., Solanki et al., 2004) which, along with other long-term solar proxies has applications to
209 paleoastrophysics, paleomagnetism and paleoclimatology (e.g., Beer et al., 2012).

210 Supplementary materials related to this article can be found online at ...

211 **Acknowledgements**

212 This work uses results obtained in research funded from the European Unions Seventh Framework Programme
213 (FP7/2007-2013) under grant agreement No 262773 (SEPServer). The High-Energy Division of Institute for Nuclear
214 Research and Nuclear Energy - Bulgarian Academy of Sciences is acknowledged for the given computational time.
215 GAK was partly supported by the Program No. 22 of presidium RAS. University of Oulu and the Academy of Finland
216 are acknowledged for partial support.

217 **Appendix A. Appendix: Details of numerical computations**

218 Numerical computations were done using the GEANT-based Monte-Carlo simulation tool Planetocosmic (Desorgher et al.,
219 2005), which traces the atmospheric cascade induced by the primary cosmic ray particles in full detail, including the
220 distribution of secondary particles. The Planetocosmic code has been recently verified (Usoskin et al., 2009) to agree
221 within $\approx 10\%$ with another commonly used Monte-Carlo package CORSIKA (Heck et al., 1998), in the sense of en-
222 ergy deposition in the atmosphere. The code simulates interactions and decays of various particles in the atmosphere
223 in a wide range of energy. For the computations, we applied a realistic spherical atmospheric model NRMLSISE-00
224 (Hedin, 1991; Picone et al., 2002). The QGSP_BIC_HP hadron interaction model has been applied with the standard
225 electromagnetic interaction model.

226 As an input for the simulations we used primary particles with fixed energy that impinge upon the top of the
227 atmosphere at the random angle isotropically from the 2π solid angle. All computations were normalized per one
228 such simulated particle. From the simulations we obtained the sum of secondary neutrons with energy within the ΔE
229 energy bin centered at the energy E_n , crossing a given horizontal level (atmospheric depth X g/cm²), weighted with

230 $|1/\cos\theta|$ (where θ is the zenith angle) to account for the geometrical factor, and divided by the energy bin width ΔE .
 231 This corresponds to the flux of secondary neutron with given energy $F(E_n, X)$ across a horizontal unit area, for the
 232 unit flux of primary cosmic rays on the top of the atmosphere. On the other hand, for quasi-stationary flux of neutrons
 233 this can be expressed as

$$F(E_n, X) \equiv n_n(E_n, X) v_n(E_n), \quad (\text{A1})$$

234 where n_n and v_n are the concentration (in $[\text{MeV cm}^3]^{-1}$) and velocity of neutrons with energy E_n at the atmospheric
 235 depth level X . Let us denote the integral columnar flux as

$$I(E_n) = \int_0^{X_m} F(E_n, X) dX, \quad (\text{A2})$$

236 where $X_m = 1033 \text{ g/cm}^2$ is the total thickness of the atmosphere. Since our direct computations were performed down
 237 to energy of neutrons $E_1 = 10 \text{ eV}$, we first computed the production of ^{14}C by these super-thermal neutrons,

$$G_1 = \sum_j \int_h \left(\int_{E_1}^{\infty} F(E_n, X) n_j(h) \sigma_j(E_n) dE_n \right) dh, \quad (\text{A3})$$

238 where the outer integral is taken over the atmospheric height h , the concentration of target nuclei $n_j(h)$ is defined as a
 239 product of the air density ρ and the content of the nuclei in a gram of air κ_j , $n_j(h) = \rho(h)\kappa_j$; $\sigma_j(E)$ is the cross-section
 240 of the corresponding reaction, and $dX = \rho(h) dh$, and summation is over target nuclei of different type (nitrogen
 241 $\kappa_{\text{N}} = 3.225 \cdot 10^{22} \text{ atom/g}$; oxygen $\kappa_{\text{O}} = 8.672 \cdot 10^{21} \text{ atom/g}$; argon $\kappa_{\text{Ar}} = 1.94 \cdot 10^{20} \text{ atom/g}$, we also accounted for the
 242 isotopic distribution within these groups). Eqs. A3 and A2 can be transformed so that

$$G_1 = \sum_j \kappa_j \int_{E_1}^{\infty} I(E_n) \sigma_j(E_n) dE_n, \quad (\text{A4})$$

243 All the cross-sections, used here, have been adopted from the Experimental Nuclear Reaction Database (EXFOR/CSISRS)
 244 <http://www.nndc.bnl.gov/exfor/exfor00.htm>.

245 We note that all the processes related to leakage of neutrons from the atmosphere (to the space or to soil) as well
 246 as their decay are accounted for in the direct simulation.

247 Monte-Carlo simulations require extensive computational time in order to trace neutrons to thermal energy, thus
 248 compromising the statistical robustness of the results. On the other hand, the fate of 10 eV neutrons can be easily
 249 modelled theoretically, because of the simplicity of the processes involved, which allows us to save computational
 250 time and improve accuracy of the computations. The main process affecting epi-thermal neutrons in air is potential
 251 elastic scattering on N and O nuclei making neutrons to lose energy. After each elastic scattering, a neutron has a
 252 uniform distribution of energy (in the laboratory frame) between its energy before the scattering E_n and αE_n (e.g.,
 253 Chapter 7.2 in Fermi, 2010). Here

$$\alpha = \frac{(A-1)^2}{(A+1)^2}, \quad (\text{A5})$$

254 where A is the mass number of the target nucleus. Then the probability for a neutron with the energy E_n (if $E_1 \leq$
 255 $E_n < E_1/\alpha$) before elastic scattering on a nuclei j to have energy E after the scattering so that $E < E_1$ is $(E_1 -$

256 $\alpha_j E_n)/(E_n(1 - \alpha_j))$. Accordingly the "flux" (in the energy domain) of neutrons crossing the energy boundary E_1 to
 257 (epi)thermal energies can be calculated as

$$N = \sum_j \int_h \int_{E_1}^{E_1/\alpha_j} F(E_n, X) n_j(X) \sigma_{\text{el},j}(E_n) \frac{E_1 - \alpha_j E_n}{E_n(1 - \alpha_j)} dE_n dh \quad (\text{A6})$$

258 or, using Eq. A2 as

$$N = \sum_j \kappa_j \int_{E_1}^{E_1/\alpha_j} I(E_n) \sigma_{\text{el},j}(E_n) \frac{E_1 - \alpha_j E_n}{E_n(1 - \alpha_j)} dE_n \quad (\text{A7})$$

259 Reactions involving neutrons are: (1) N14(n,p)C14; (2) O17(n, α)C14; (3) N14(n, γ)N15; (4) O16(n, γ)O17; (5)
 260 O18(n, γ)O19 and (6) Ar40(n, γ)Ar41. Note that only reactions (1) and (2) lead to production of ^{14}C while others
 261 simply provide a sink for neutrons. Cross-sections of neutron capture in all these reactions for energies below 10 eV
 262 can be expressed as

$$\sigma_j = \frac{B_j}{v_n(E_n)}, \quad (\text{A8})$$

263 where B_j is a constant. Accordingly, the ^{14}C production by these neutrons can be calculated as

$$G_2 = N \frac{B_1 \cdot \kappa_{\text{N14}} + B_2 \cdot \kappa_{\text{O17}}}{\sum_j B_j \cdot \kappa_j} \quad (\text{A9})$$

264 The bulk of radiocarbon ^{14}C is produced via reaction (1) and about 0.001% in reaction (2). This is the main channel
 265 (95.8%) of the neutron sink. We have also considered leakage of neutrons from the upper atmospheric layers and decay
 266 of neutrons during their thermalization. These processes appear to be unimportant. In addition, we also computed
 267 possible contribution of secondary and primary protons to ^{14}C production via spallation reactions (e.g., O16(p,X)C14).
 268 These reactions are responsible for a negligible contribution to the total production.

269 Then the final production of ^{14}C in the atmosphere by secondary neutrons corresponding to the primary cosmic
 270 ray particle with given energy is the sum of G_1 and G_2 and forms a point in the yield function Y/π .

271 References

- 272 Adriani, O., Barbarino, G. C., Bazilevskaia et al., 2011. PAMELA Measurements of Cosmic-Ray Proton and Helium Spectra. *Science* 332, 69–72.
 273 Alanko-Huotari, K., Usoskin, I. G., Mursula, K., Kovaltsov, G. A., 2007. Cyclic variations of the heliospheric tilt angle and cosmic ray modulation.
 274 *Adv. Space Res.* 40, 1064–1069.
 275 Alcaraz, J., Alpat, B., Ambrosi, G., et al., 2000a. Cosmic protons. *Phys. Lett. B* 490, 27–35.
 276 Alcaraz, J., Alpat, B., Ambrosi, G., et al., 2000b. Helium in near Earth orbit. *Phys. Lett. B* 494, 193–202.
 277 Bard, E., Raisbeck, G., Yiou, F., Jouzel, J., 1997. Solar modulation of cosmogenic nuclide production over the last millennium: comparison
 278 between ^{14}C and ^{10}Be records. *Earth Planet. Sci. Lett.* 150, 453–462.
 279 Beer, J., 2000. Neutron monitor records in broader historical context. *Space Sci. Rev.* 93, 107–119.
 280 Beer, J., McCracken, K., von Steiger, R., 2012. *Cosmogenic Radionuclides: Theory and Applications in the Terrestrial and Space Environments.*
 281 Springer, Berlin.
 282 Bolin, B., Degens, E., Kempe, S., Ketner, P. e., 1979. *The global carbon cycle.* John Wiley and Sons, New York.
 283 Burger, R., Potgieter, M., Heber, B., 2000. Rigidity dependence of cosmic ray proton latitudinal gradients measured by the ulysses spacecraft:
 284 Implications for the diffusion tensor. *J. Geophys. Res.* 105, 27447–27456.

285 Castagnoli, G., Lal, D., 1980. Solar modulation effects in terrestrial production of carbon-14. *Radiocarbon* 22, 133–158.

286 Clem, J. M., Bieber, J. W., Evenson, P., Hall, D., Humble, J. E., Duldig, M., 1997. Contribution of obliquely incident particles to neutron monitor
287 counting rate. *J. Geophys. Res.* 102, 26919–26926.

288 Damon, P., Sternberg, R., 1989. Global production and decay of radiocarbon. *Radiocarbon* 31, 697–703.

289 Dergachev, V., Veksler, V., 1991. Application of the Radiocarbon Method for Studies of the Environment in the Past. A.F. Ioffe Phys-Tech Inst.,
290 Acad. Sci. USSR, Leningrad, USSR (in Russian).

291 Desorgher, L., Flückiger, E. O., Gurtner, M., Moser, M. R., Büttikofer, R., 2005. Atmocosmics: a Geant 4 Code for Computing the Interaction of
292 Cosmic Rays with the Earth's Atmosphere. *Intern. J. Modern Phys. A* 20, 6802–6804.

293 Dorman, L., 2004. *Cosmic Rays in the Earth's Atmosphere and Underground*. Kluwer Academic Publishers, Dordrecht, Netherlands.

294 Dorman, L., 2009. *Cosmic Rays in Magnetospheres of the Earth and other Planets*. Springer, New York.

295 Elsasser, W., Nay, E., Winkler, J., 1956. Cosmic-ray intensity and geomagnetism. *Nature* 178, 1226–1227.

296 Fermi, E., 2010. *Neutron Physics for Nuclear Reactions: Unpublished writings by Enrico Fermi* (Eds. Esposito, S., Pisanti, O.). World Scientific
297 Publishing, Singapore.

298 Garcia-Munoz, M., Mason, G., Simpson, J., 1975. The anomalous ^4He component in the cosmic-ray spectrum at below approximately 50 mev per
299 nucleon during 1972-1974. *Astrophys. J.* 202, 265–275.

300 Geant4 Collaboration, Agostinelli, S., Allison, J., Amako, K., et al., 2003. Geant4-a simulation toolkit. *Nucl Instr. Meth. Phys. Res. A* 506,
301 250–303.

302 Goslar, T., 2001. Absolute production of radiocarbon and the long-term trend of atmospheric radiocarbon. *Radiocarbon* 43, 743–749.

303 Heck, D., Knapp, J., Capdevielle, J., Schatz, G., Thouw, T., 1998. Corsika: A monte carlo code to simulate extensive air showers. In: FZKA 6019.
304 Forschungszentrum, Karlsruhe.

305 Hedin, A. E., 1991. Extension of the MSIS thermosphere model into the middle and lower atmosphere. *J. Geophys. Res.* 96, 1159–1172.

306 Herbst, K., Kopp, A., Heber, B., Steinhilber, F., Fichtner, H., Scherer, K., Matthiä, D., 2010. On the importance of the local interstellar spectrum
307 for the solar modulation parameter. *J. Geophys. Res.* 115, D00I20.

308 Hudson, H. S., 2010. Solar flares add up. *Nature Phys.* 6 (9), 637–638.

309 Korff, S., Mendell, R., 1980. Variations in radiocarbon production in the Earth's atmosphere. *Radiocarbon* 22 (2), 159–165.

310 Korte, M., Constable, C., Donadini, F., Holme, R., 2011. Reconstructing the Holocene geomagnetic field. *Earth Planet. Sci. Lett.* 312, 497–505.

311 Kovaltsov, G. A., Usoskin, I. G., 2010. A new 3D numerical model of cosmogenic nuclide ^{10}Be production in the atmosphere. *Earth Planet. Sci.*
312 *Lett.* 291, 182–188.

313 Kromer, B., 2009. Radiocarbon and dendrochronology. *Dendrochronologia* 27 (1), 15–19.

314 Lal, D., 1988. Theoretically expected variations in the terrestrial cosmic-ray production rates of isotopes. In: G. Cini Castagnoli (Ed.), *Solar-
315 Terrestrial Relationships and the Earth Environment in the last Millennia, Proceedings of the International School of Physics "Enrico Fermi",
316 Course XCV*. North-Holland Publishing Company, Amsterdam, The Netherlands, pp. 216–233.

317 Lal, D., Suess, H., 1968. The radioactivity of the atmosphere and hydrosphere. *Ann. Rev. Nuc. Sci.* 18, 407–434.

318 LaViolette, P. A., 2011. Evidence for a solar flare cause of the pleistocene mass extinction. *Radiocarbon* 53 (2), 303–323.

319 Light, E. S., Merker, M., Verschell, H. J., Mendell, R. B., Korff, S. A., 1973. Time dependent worldwide distribution of atmospheric neutrons and
320 of their products. 2. Calculation. *J. Geophys. Res.* 78, 2741–2762.

321 Lingenfelter, R., 1963. Production of carbon 14 by cosmic-ray neutrons. *Rev. Geophys. Space Phys.* 1, 35–55.

322 Lingenfelter, R., Ramaty, R., 1970. Astrophysical and geophysical variations in c-14 production. In: Olsson, I. (Ed.), *Proc. 12th Nobel symposium,
323 Radiocarbon variations and absolute chronology*. John Wiley & Sons, NY, pp. 513–537.

324 Lockwood, J. A., Webber, W. R., Oct. 1996. Comparison of the rigidity dependence of the 11-year cosmic ray variation at the earth in two solar
325 cycles of opposite magnetic polarity. *J. Geophys. Res.* 101, 21573–21580.

326 Masarik, J., Beer, J., 1999. Simulation of particle fluxes and cosmogenic nuclide production in the earth's atmosphere. *J. Geophys. Res.* 104,
327 12,099–12,111.

328 Masarik, J., Beer, J., 2009. An updated simulation of particle fluxes and cosmogenic nuclide production in the Earth's atmosphere. *J. Geophys.*
329 *Res.* 114, D11103.

330 Masarik, J., Reedy, R. C., 1995. Terrestrial cosmogenic-nuclide production systematics calculated from numerical simulations. *Earth Planet. Sci.*
331 *Lett.* 136, 381–395.

332 McCracken, K., McDonald, F., Beer, J., Raisbeck, G., Yiou, F., 2004. A phenomenological study of the long-term cosmic ray modulation, 850-1958
333 *ad. J. Geophys. Res.* 109 (A18), 12103.

334 Muscheler, R., Joos, F., Beer, J., Müller, S., Vonmoos, M., Snowball, I., 2007. Solar activity during the last 1000 yr inferred from radionuclide
335 records. *Quater. Sci. Rev.* 26, 82–97.

336 Nakamura, K., Hagiwara, K., Hikasa, K., et al., 2010. REVIEW OF PARTICLE PHYSICS. *J. Phys. G* 37 (7A), 1–1422.

337 O'Brien, K., 1979. Secular variations in the production of cosmogenic isotopes in the earth's atmosphere. *J. Geophys. Res.* 84, 423–431.

338 O'Brien, K., 2008. Limitations of the use of the vertical cut-off to calculate cosmic-ray propagation in the earth's atmosphere. *Radiation Protection*
339 *Dosimetry* 128, 259–260.

340 O'Brien, K., 2010. The Local All-particle Cosmic-ray Spectrum. *Astrophys. J.* 716, 544–549.

341 O'Brien, K., de la Zerda Lerner, A., Shea, M., D.F., S., 1991. The production of cosmogenic isotopes in the earth's atmosphere and their inventories.
342 In: Sonett, C., Giampapa, M., Matthews, M. (Eds.), *The Sun in Time*. University of Arizona Press, Tucson, U.S.A., pp. 317–342.

343 Picone, J. M., Hedin, A. E., Drob, D. P., Aikin, A. C., 2002. NRLMSISE-00 empirical model of the atmosphere: Statistical comparisons and
344 scientific issues. *J. Geophys. Res.* 107, Cite ID 1468.

345 Reimer, P. J., Baillie, M. G. L., Bard, E., et al., 2009. INTCAL09 and Marine09 radiocarbon age calibration curves, 0-50000 years cal BP.
346 *Radiocarbon* 51 (4), 1111–1150.

347 Simpson, J. A., 1983. Elemental and Isotopic Composition of the Galactic Cosmic Rays. *Annual Rev. Nuc. Part. Sci.* 33, 323–382.

348 Snowball, I., Muscheler, R., 2007. Palaeomagnetic intensity data: an achilles heel of solar activity reconstructions. *Holocene* 17, 851–859.

349 Solanki, S., Usoskin, I., Kromer, B., Schüssler, M., Beer, J., 2004. Unusual activity of the sun during recent decades compared to the previous
350 11,000 years. *Nature* 431, 1084–1087.

351 Steinhilber, F., Abreu, J. A., Beer, J., 2008. Solar modulation during the Holocene. *Astrophys. Space Sci. Trans.* 4, 1–6.

352 Stuiver, M., Braziunas, T., 1989. Atmospheric ^{14}C and century-scale solar oscillations. *Nature* 338, 405–408.

353 Stuiver, M., Quay, P., 1980. Changes in atmospheric carbon-14 attributed to a variable sun. *Science* 207, 11–19.

354 Tylka, A., Dietrich, W., 2009. A new and comprehensive analysis of proton spectra in ground-level enhanced (gle) solar particle events. In: 31th
355 International Cosmic Ray Conference. Universal Academy Press, Lodz, Poland.

356 Usoskin, I., Kovaltsov, G., 2008. Production of cosmogenic ^7Be isotope in the atmosphere: Full 3D modelling. *J. Geophys. Res.* 113.

357 Usoskin, I., Solanki, S., Kovaltsov, G., Beer, J., Kromer, B., 2006. Solar proton events in cosmogenic isotope data. *Geophys. Res. Lett.* 33, L08107.

358 Usoskin, I. G., Alanko-Huotari, K., Kovaltsov, G. A., Mursula, K., 2005. Heliospheric modulation of cosmic rays: Monthly reconstruction for
359 1951–2004. *J. Geophys. Res.* 110, A12108.

360 Usoskin, I. G., Bazilevskaya, G. A., Kovaltsov, G. A., 2011. Solar modulation parameter for cosmic rays since 1936 reconstructed from ground-
361 based neutron monitors and ionization chambers. *J. Geophys. Res.* 116, A022104.

362 Usoskin, I. G., Desorgher, L., Velinov, P., Storini, M., Flückiger, E. O., Büttikofer, R., Kovaltsov, G. A., 2009. Ionization of the earth's atmosphere
363 by solar and galactic cosmic rays. *Acta Geophys.* 57, 88–101.

364 Usoskin, I. G., Solanki, S. K., Kovaltsov, G. A., 2007. Grand minima and maxima of solar activity: new observational constraints. *Astron.*
365 *Astrophys.* 471, 301–309.

366 Webber, W., Higbie, P., 2003. Production of cosmogenic be nuclei in the earth's atmosphere by cosmic rays: Its dependence on solar modulation
367 and the interstellar cosmic ray spectrum. *J. Geophys. Res.* 108, 1355.

368 Webber, W., Higbie, P., McCracken, K., 2007. Production of the cosmogenic isotopes ^3H , ^7Be , ^{10}Be , and ^{36}Cl in the earth's atmosphere by solar and
369 galactic cosmic rays. *J. Geophys. Res.* 112.

370 Webber, W. R., Higbie, P. R., 2009. Galactic propagation of cosmic ray nuclei in a model with an increasing diffusion coefficient at low rigidities:

371 A comparison of the new interstellar spectra with Voyager data in the outer heliosphere. *J. Geophys. Res.* 114, A02103.

Table A.1: Normalized yield functions Y_p/π and Y_α/π of the atmospheric columnar ^{14}C production (in atoms sr) by a nucleon of primary cosmic protons and α -particles, respectively, with the energy given in GeV/nuc. For energy above 20 GeV/nuc, an α -particle is considered to be identical to four protons.

E (GeV/nuc)	0.1	0.3	0.5	0.7	1	3	7	10	19	49	99	499	999
proton	0.025	0.26	0.72	1.29	2.07	5.19	8.32	9.72	12.40	17.45	23.24	48.30	72.73
$\alpha/4$	0.036	0.38	0.89	1.55	2.16	4.18	7.17	8.67	12.40	17.45	23.24	48.30	72.73

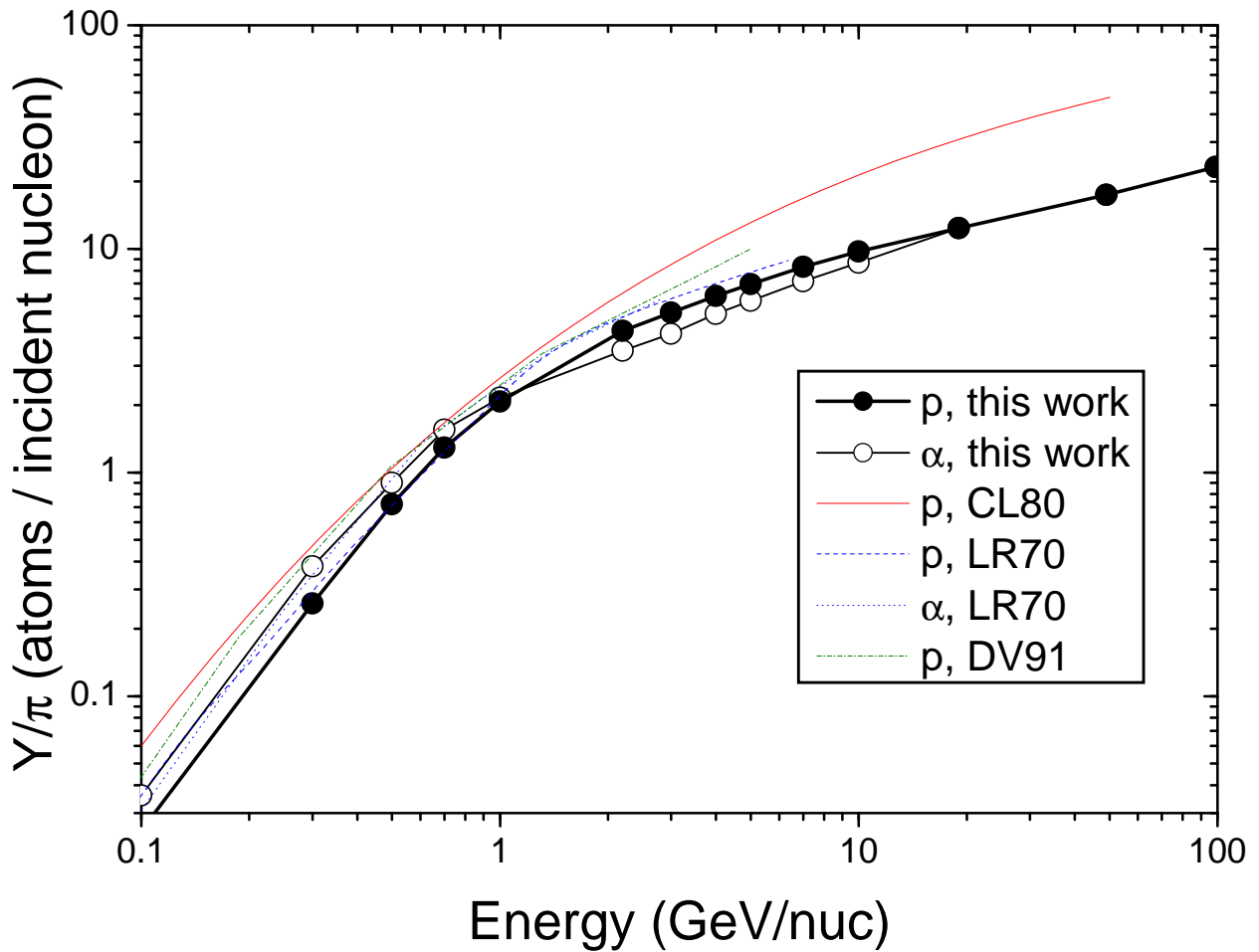


Figure A.1: Yield function Y/π of ^{14}C production in the Earth's atmosphere by primary cosmic rays protons and α -particles (as denoted by "p" and " α " in the legend, respectively) with given energy per nucleon. Different curves correspond to the present work (Table A.1) and earlier models (CL80 - Castagnoli and Lal, 1980), (LR70 - Lingenfelter and Ramaty, 1970) and (DV91 - Dergachev and Veksler, 1991), as denoted in the legend.

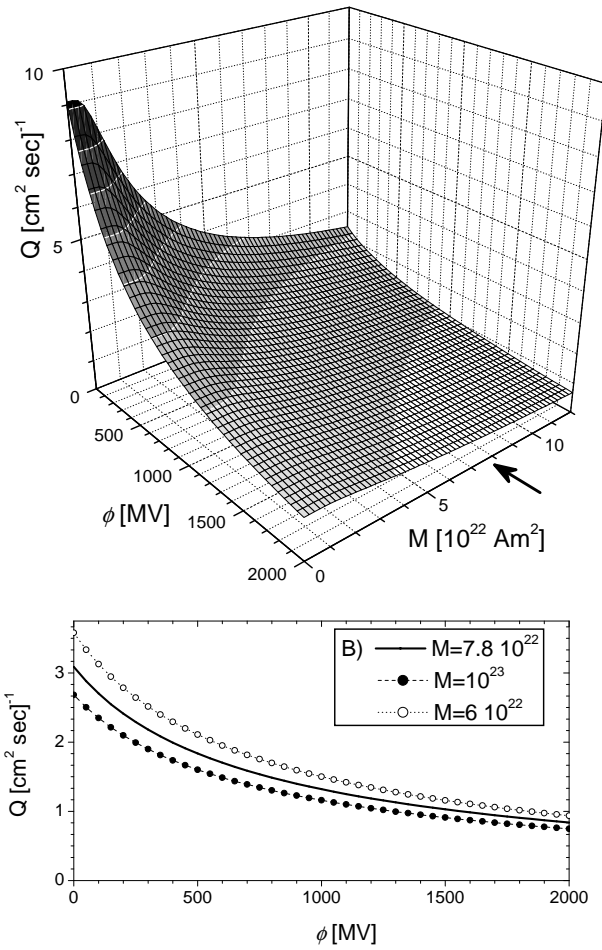


Figure A.2: The global production of ^{14}C as function of the modulation potential ϕ and the geomagnetic dipole moment M . The present value of $M = 7.8 \cdot 10^{22} \text{ A m}^2$ is indicated by the thick arrow. The lower panel shows three cross-sections of the upper panel corresponding to the present value as well as to the maximum and minimum values of M over the past millennia, as indicated in the legend. Digital table for this plot is available at electronic supplement for this paper.

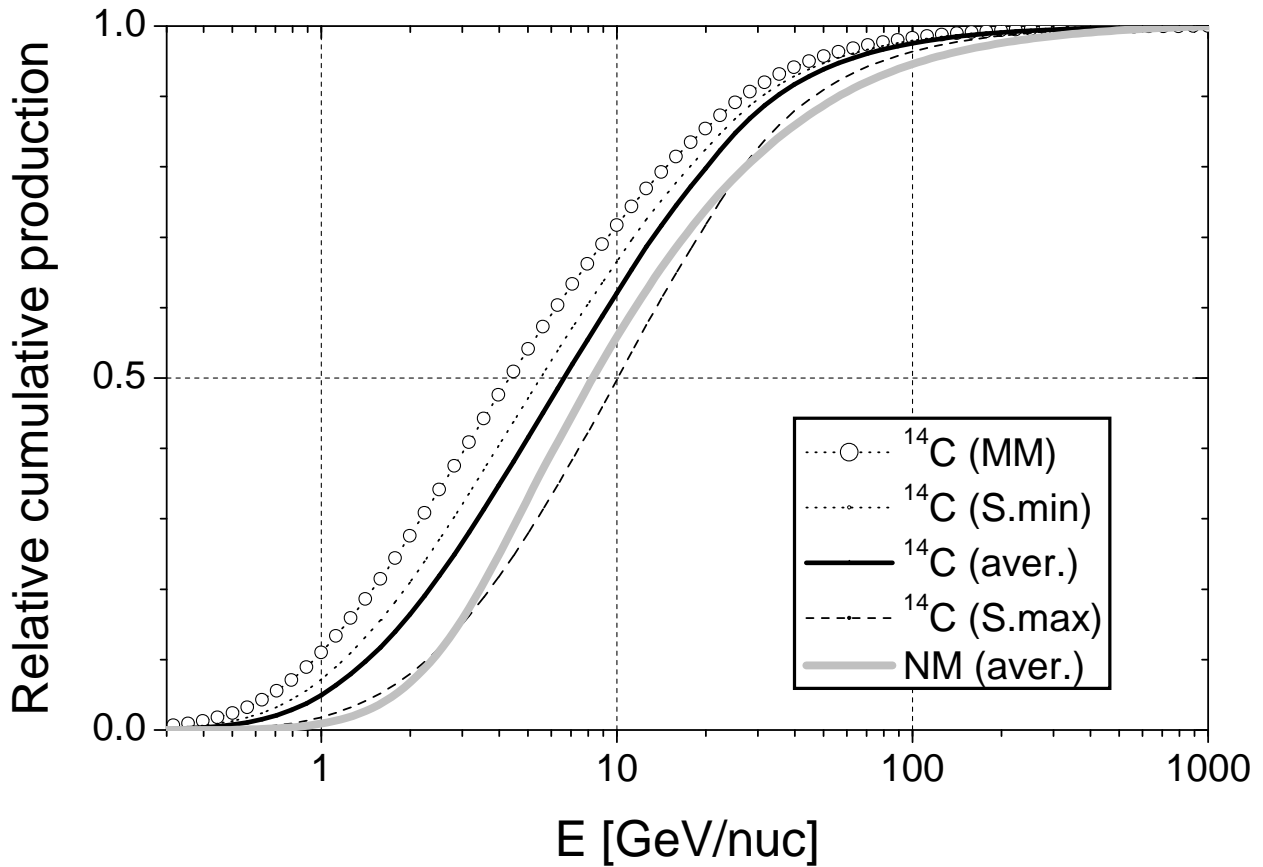


Figure A.3: Relative cumulative production of ^{14}C (fraction of the total production) as a function of the primary cosmic ray energy for different conditions: average solar activity (solid "aver." curve), solar maximum ($\phi = 1200$ MV, dashed "S.max" curve), solar minimum ($\phi = 300$ MV, dotted "S.min" curve), Maunder minimum ($\phi = 100$ MV, circled "MM" curve). The thick grey curve corresponds to a polar sea-level neutron monitor. All curves are shown for the modern Earth magnetic field.

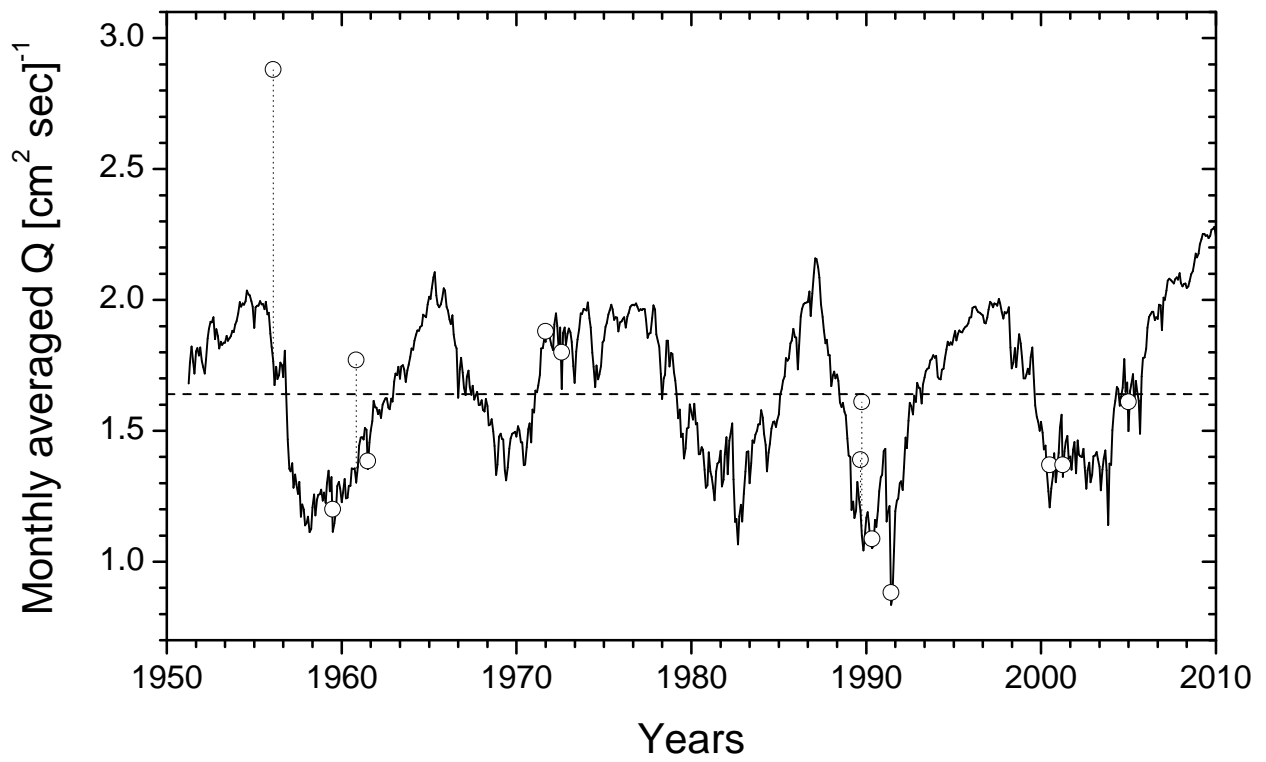


Figure A.4: Monthly averaged global production rates of ^{14}C since 1951 calculated using cosmic rays data from the world network of neutron monitors and our calculated yield function. Open circles correspond to months with major solar energetic particle events.

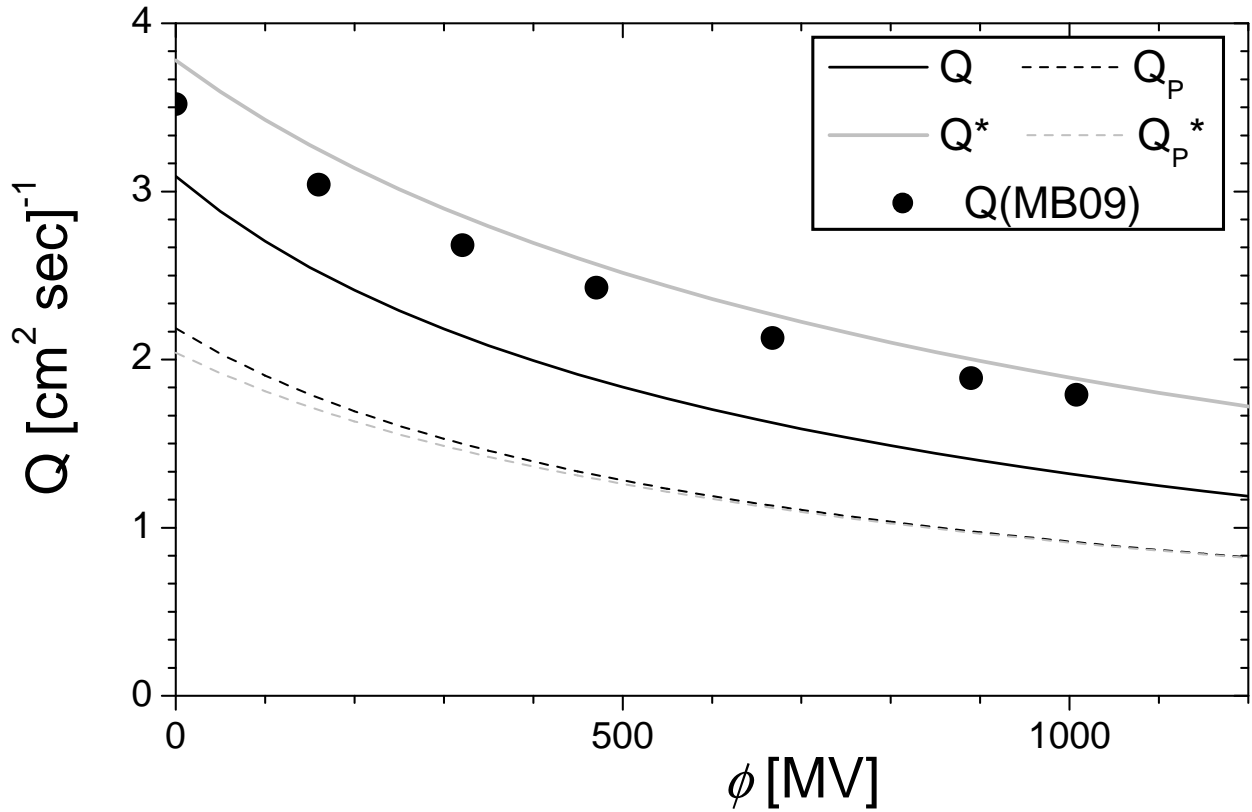


Figure A.5: Comparison of the global ^{14}C production rates, computed by different models as function of the modulation potential for the modern geomagnetic field. Big dots correspond to the original results by Masarik and Beer (2009). Curves are computed using our calculated yield function (Table A.1) and applying different cosmic rays spectra. Black curves (Q values) are calculated using the present results, while grey curves (Q^* values) are calculated using our yield function but GCR spectra as used by Masarik and Beer (2009). Solid and dashed lines correspond to the total production and to production only by primary protons, respectively.

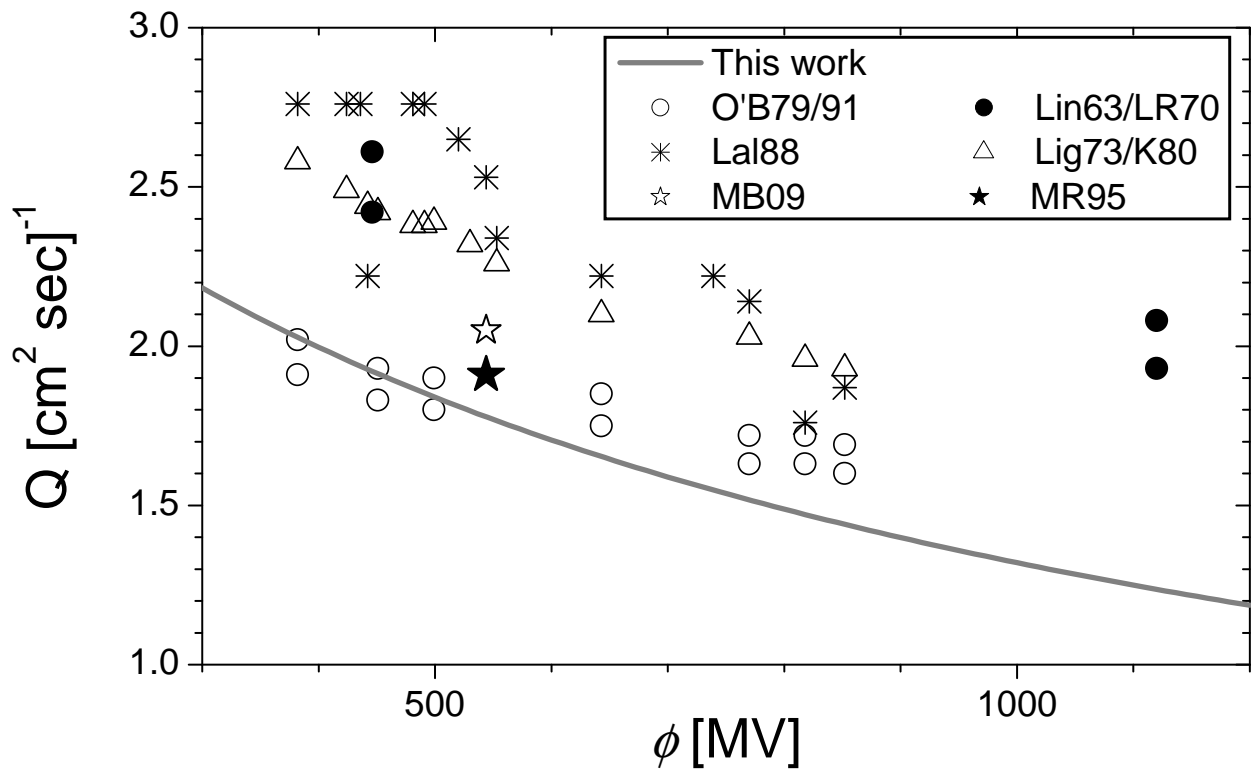


Figure A.6: Global ^{14}C production as function of the modulation potential ϕ as defined in Usoskin et al. (2011). The thick grey curve presents the present work's results. Symbols corresponds to earlier works: O'B79/91 (Tab. 7 in O'Brien, 1979; O'Brien et al., 1991); Lin63/LR70 (Tab. 1 in Lingenfelter, 1963; Lingenfelter and Ramaty, 1970); Lal88 (Tabs. I and III in Lal, 1988); Lig73 (Tab. 6 in Light et al., 1973), K80 (Tab. 1 in Korff and Mendell, 1980); MB09 (Tab. 3 in Masarik and Beer, 2009); MR95 (Tab. 1 in Masarik and Reedy, 1995).